Fabrication of Biologically Active Fish Bone Derived Hydroxyapatite and Montmorillonite Blended Sodium Alginate Composite for *In-vitro* Drug Delivery studies

A Fiaz Ahamed
Murugaiyan Manimohan
N Kalaivasan (nkvvasan78@gmail.com)
Thanthai Periyar Government Institute of Technology

Research Article

Keywords: Fish-bone waste, hydroxyapatite, Biopolymer composite, drug release, antioxidant, antidiabetic

Posted Date: March 11th, 2022

DOI: https://doi.org/10.21203/rs.3.rs-1427968/v1

Abstract

Fishbone comprising hydroxyapatite (bio-ceramic) is regularly viewed as a natural resource for biological and pharmaceutical applications. In this study, hydroxyapatite has been prepared from fishbone waste using thermal calcination method. The composite hydroxyapatite-montmorillonite-sodium alginate was synthesized by co-precipitation method. Various functional groups of biocomposite were characterised using Fourier Transform infrared spectroscopy (FT-IR). Thermal gravimetric analysis (TGA) and X-ray diffraction studies were exhibited the thermal stability and crystallinity of biocomposite respectively. The morphological surface of composites was studied using scanning electron microscopy (SEM). The synthesized composite was designed to study the enhanced biological potential such as antibacterial, antioxidant, antidiabetic, drug loading and the drug releasing ability. Antioxidant and anti-diabetic analysis of composite were studied using Phosphomolybdenum and α-Amylase inhibitory method respectively. The drug releasing ability of compounds (Doxorubicin and Curcumin) were investigated by UV–spectrophotometry method at different pH medium (pH = 5.5, 6.8 and 7.4). Additionally, *In-vitro* kinetic studies were carried out on composite to determine the drug releasing ability of doxorubicin and curcumin.

Introduction

Osteosarcoma bone tumour can metastasize to infiltrate the bones, resulting in bone defects and posing a critical threat to human health [1]. Surgical treatment, chemotherapy, and radiotherapy are currently the most effective treatments for bone tumours. In chemotherapy, patients ensuing excessive intake of drugs leads to nausea, diarrhoea, hair loss, vomiting and killing of healthy cells in the human body [2]. Due to the repercussions of chemotherapy, limiting the dosage of the drug resulted in diminishing anti-cancer efficacy. Drug carriers are used to control the drug delivery and provide the effective chemotherapy as well as minimal side effects in the treatment [3].

The chemotherapy drugs doxorubicin (DOX) and Curcumin (Cur) have been used in the treatment of osteosarcoma to inhibit the growth of tumour cells [4]. Though, excessive release of drug contradicts as significant changes in cytotoxicity causes harm to normal cells [5]. In order to attain the long-term potent release and permit sustained release of drugs, suitable carrier materials are needed that are of appropriate biocompatibility [6]. Recent researches have been focus on design, preparation and improvement of associated drug carriers.

Hydroxyapatite (HA) has received increasing attention as a potential material for drug delivery carriers because of its nontoxicity, biocompatibility, and charge groups, which make it possible to load drugs onto the material [7, 8]. Hydroxyapatite also promotes osteogenesis in addition to drug delivery, it may be an appropriate candidate to prevent tumour recurrence after osteosarcoma resection and nurture bone regeneration [9]. The raw materials for producing hydroxyapatite can also be obtained from natural calcium sources like mussel shells and eggshells [10, 11]. In addition to the above, fishbone is considered as the inexpensive and easily accessible source of Hydroxyapatite. It is regarded as a non-essential waste

material obtained from by-product of the seafood industry [12]. A large amount of fishbone waste is generated each year due to increase in fish consumption around the world. Globally, approximately 970–2700 billion tons of fish have been catching with 450–1000 billion being consumed by humans [13]. Furthermore, natural and conventional synthetic stoichiometric hydroxyapatite has significantly different properties [14]. Naturally derived hydroxyapatite provides magnesium, zinc and strontium ions [15]. Moreover, natural hydroxyapatite contains considerable amounts of carbonates and trace elements, thereby stimulating the biological activity of osteoblasts in the body [16]. Because of being too brittle due to ceramic nature, it is necessary to develop biomaterial surfaces to attain drug delivery properties by increasing percentage of drug holding and avoiding burst release [17].

Sodium Alginate (SA) is a class of biopolymer, derives from marine algae, brown seaweeds and soil bacteria, it is called linear polysaccharide [18]. The properties of composites such as thickening, gelling and film forming ability makes better efficacies in many industrial fields including pharmaceutical, medical, paper, leather, food, immobilized catalysts and textile printing [19, 20]. Biocompatibility, biodegradability, less toxicity and hydrophilicity of the alginate are highly suitable for drug delivery applications. Hydroxyapatite along with alginate increased the cell attachment in the inner parts and offers a suitable choice of composite for bone tissue engineering [21]. Usually polysaccharides release matrixes that have high water content and the release of low molecular weight drugs is not effectively controlled due to the high rate of release and the obvious burst release. Thus compared to protein drugs, controlled release of low molecular weight anticancer drugs through encapsulation in polysaccharides such as alginate has certain limitations [22]. Since, many research concerning the use of clays to perform specific tasks such as delay or target drug release, improve drug dissolution, increase drug stability, and modify drug delivery patterns. Among clays, Montmorillonite (MMT) has drawn considerable attention due to its high specific surface area, swelling capacity and cationic exchange capacity makes modification of polymer. This tends to expand the applications in various fields such as adsorption and sensor etc., [23, 24]. Also, controlled release properties, oral bioavailability, gastrointestinal cross-ability and mucoadhesiveness make it suitable for pharmaceutical applications [25].

The ultimate aim of this work is to prepare a bio-composite derived from natural hydroxyapatite and evaluate a new drug delivery material and carry out in-vitro efficacy of the prepared bio-composite material in biological applications including antimicrobial, anti-inflammatory, antioxidant and antidiabetic. To the best of our knowledge, so far there are no considerable works that have been done on hydroxyapatite / montmorillonite/sodium alginate composite prepared from fishbone and used for drug delivery.

Material And Methods

Sodium alginate (SA) (medium viscosity), medium molecular weight 1,30,000 g/mol, Montmorillonite clay (MMT), Doxorubicin hydrochloride (DOX), Curcumin (CUR), Methanol, Ethanol, Acetone, Toluene, Sodium hydroxide, Ammonium hydroxide, Dimethylsulphoxide (DMSO), Dimethylformamide (DMF) and

Scomberomorus Guttatus (Seer fish) bone collected from Patinapakkam, Chennai, Tamilnadu, India. All the chemicals were analytical grade and purchased from Sigma Aldrich, India.

2.1Preparation of Hydroxyapatite (HA)

Fishbone (1 kg) was boiled in water at 150 ^{o}C for about 30 minutes until the flesh and skin were eliminated from the bone. Then, it is allowed to react with 10 % butanol for 48 h and then it is treated with a strongly alkaline medium and followed by acetone to remove the fat, proteins, lipids, oils and other organic contents. Furthermore, the product was washed with distilled water and filtered through a suction pump until the pH was neutral. The obtained fish bone was dried in a hot air oven for 5 hours at 80 ºC. The product was crushed and ground into powder using ball milling before the calcination process. 2 g of fishbone powder and phosphate buffer mixture was placed in a silica coated crucible and subjected to a temperature of 900 °C for 6 hours in an electrical muffle furnace at a ramp rate of 15 ^{o}C / min and then allowed to cool to room temperature. The white product HA was obtained and pulverized into a fine powder.

2.2 Synthesis of Hydroxyapatite/Montmorillonite (HA/MMT) composite

A required amount of montmorillonite clay was ground and dried to 120 ºC for 24 h and stored in desiccators prior to use. In 100 mL of deionized water, 0.5 g of montmorillonite clay was dispersed and sonicated using an ultrasonicator at 80 watts for 30 min. Then, the 1 g of as-prepared hydroxyapatite was added slowly in 100 mL of montmorillonite suspension, agitated under magnetic stirrer for 2 hours, followed by sonication for 30 min. The obtained suspension was centrifuged and slurry was separated by discarding the supernatant. Afterwards, it was washed twice with distilled water and then ethanol to eradicate the impurities and unreacted substance. Furthermore, it was allow to dried in a vacuum oven at 60°C for 5h and the resulting HA/MMT composite was ground well into powder.

2.3 Synthesis of Hydroxyapatite/Sodium alginate (HA / SA) composite

Sodium alginate (0.5g) was dissolved in distilled water (100 ml) at 60 °C and obtained viscous solution was allowed to cool to room temperature. Then, 1g of as prepared hydroxyapatite was added slowly to viscous alginate solution under constant stirring using magnetic stirrer at 1000 rpm for 1h. After centrifuging the obtained suspension, the slurry was separated by discarding the supernatant. Then, it was washed with distilled water and then with ethanol to remove any impurities. The obtained HA / SA composite was recovered by drying in a vacuum oven at 60°C for 5 h and ground well into powder (**Scheme.1**).

2.4 Synthesis of Hydroxyapatite/Montmorillonite/Sodium alginate composite (HA/MMT/SA)

0.5g of Sodium alginate was dissolved in distilled water (100 ml) at 60 °C and was cooled to room temperature (25 °C). After, 1 g of as prepared HA/MMT was dispersed stirred and followed by the sonication for 15 min. Then, prepared viscous alginate solution was added gradually into resulting

HA/MMT clay suspension was continuously stirred under magnetic stirrer at 1000 rpm for 1 hour. Slurry was separated from the suspension by centrifugation and washed with distilled water and ethanol to make free from impurity substances. The resulting HA/MMT/SA composite was then dried in a vacuum oven at 60°C for 5 h and ground finely into powder (**Scheme.1**).

2.5 Composite Characterization

2.5.1 Fourier Transform Infra-red (FT-IR) analysis

Prepared compounds were studied using Fourier Transform Infra-red analysis. The compounds were characterised at the range of 400 – 4000 cm^{-1} using the Perkin Elmer Spectrum Version 10.4.00, KBr pellet method.

2.5.2 Porosity

The percentage of spaces or air voids (pores) within a solid material in the dry state of the polymer composite represents the percentage of porosity (ϕ) and it was estimated from their densities. The weights of polymer and their derivatives were measured using the formula.

$$\text{Dry state porosity } (\varphi) = \frac{(1 - Vma)}{Vb} \times 100 \quad \ldots\ldots\ldots\ldots\ldots\ldots\ldots\ldots (1)$$

Where Vb and Vma are the total volume of the compound and the volume of matrix respectively.

2.5.3 X-ray diffraction (XRD) studies

Wide-angle X-ray diffractogram and Small X-ray diffractogram were recorded for prepared samples using 2.2KW Cu-anode ceramic tube, Lynx Eye Detector (Silicon strip detector technology) & Scintillation Detector (for low angle XRD analysis) D8 advance, Bruker, Germany. The XRD spectra were analysed with an applied voltage of 40 kV with a current of 30 mA, Cu Kα radiation (λ=0.15406 nm), scan rate of 0.02˚ per second and the angles from 0˚ to 10˚ (small angle) and 10˚ to 90˚ (wide angle) were analysed for the samples. The crystalline size was calculated by using following equation

$$\text{Crystalline Size } D = \frac{k.\lambda}{\beta \cos\theta} \quad \ldots\ldots\ldots\ldots\ldots\ldots\ldots\ldots (2)$$

D - Crystallite size, λ - wavelength of X-rays, *k* - Scherrer constant and β - full width at half maximum FWHM (radian).

2.5.4 Thermal gravimetric - Differential thermal (TGA-DTA) analysis

TGA-DTA curves of compounds were analysed with 2.2 mg of sample in the alumina pan and the heating rate of 20˚ C / min with the flow of nitrogen gas 100 mL /min. The TGA-DTA curves were recorded for prepared composites using SDT Q600, TA Instruments, USA.

2.5.5 Field Emission Scanning electron microscope (FESEM) analysis

The surface morphologies were studied for prepared hydroxyapatite and their composite samples and SEM images of recorded using ZEISS SIGMA Field Emission Scanning Electron Microscope. The composite were coated with gold and palladium using QUORUM Sputter Coater sc7620 prior to analysis.

2.5.6 Energy Dispersive Spectroscopic (EDAX) analysis

The EDAX spectra were analyzed for the percentage ratios of metal ions, carbon, nitrogen, oxygen, and other elements present in the synthesized hydroxyapatite-montmorillonite-biopolymer composite and spectra were recorded using Thermo Fisher Scientific FEI Company of USA.

2.6 Antibacterial activity (Agar plate method)

The antibacterial activities were studied by the agar plate method for prepared biocomposite derivatives. About 10 mg of test samples HA and their derivatives were dissolved in 10 mL of dimethyl sulphoxide (DMSO) with a concentration of 10 mg/10 mL, respectively. The antibacterial activities were done to compare the efficacy of the HA and their composites with different dosages such as 50 µL, 100 µL, 150 µL, 200 µL, and 250 µL of the stock solution. The gram-positive bacteria and gram-negative bacteria such as *S.aureus, B. Subtilis* and *E.coli, P.aeruginosa* respectively were chosen due to clinical and pharmacological importance **[26]**. The prepared bacterial stock cultures were incubated using agar nutrient and potato dextrose agar (PDA) medium (Microcare laboratory, Surat, India), respectively for 24 h at 37 °C. After the incubation, the cultures were refrigerated at 4 °C. Bacterial strains *E.coli, P.aeruginosa S.aureus* and *B.subtilis* were grown in the nutrient broth at 37 °C and were maintained on nutrient agar slants at 4 °C. Similarly, the yeasts and molds were grown in sabouraud dextrose agar and PDA media at 28 °C. Finally, grown bacterial stock cultures were maintained at 4 °C. Ampicillin was used as a reference drug **[27]**.

2.7 Total antioxidant studies (Phosphomolybdenum method)

Wound and damaged cells are repaired by the antioxidant materials. Hence, antioxidants play important role in human cell proliferation and development. The total antioxidant studies were carried out through the phosphomolybdenum method **[28]**. About 0.3 ml of test samples and standard drug vitamin C at various concentrations such as 10 µg/mL, 50 µg/mL, 100 µg/mL, 250 µg/mL and 500µg/mL were mixed with 3 mL of phosphomolybdenum reagent (0.6 mol M H_2SO_4, 28 mM Na_3PO_4 and 4 mM $(NH_4)_2\,MoO_4$). To ensure proper diffusion of the phosphomolybdenum reagent, reaction mixture was incubated in a water bath at 95 °C for 90 minutes. The total antioxidant activity of the composite, as well as that of the vitamin C standard drug, was evaluated at 695 nm using a UV-spectrometer. The total antioxidant activities of the composite were measured in terms of percentage using the following formula

$$\text{Inhibition \%} = \left[\frac{\text{Abs. Cont.} - \text{Abs. Sam.}}{\text{Abs. Cont.}}\right] \times 100 \quad \ldots\ldots\ldots\ldots\ldots\ldots\ldots\ldots (3)$$

where Abs. Cont. and Abs. Sam. are the absorbance of control and absorbance of extract respectively.

2.8 Pancreatic α-amylose inhibitory assay (McCue and Shetty method)

The antidiabetic (α-Amylase inhibitory) activities of synthesized biocomposite derivatives were studied using a modified method by McCue and Shetty **[29]**. The α-Amylase inhibitory studies were performed for the test samples and the standard drug acarbose at various concentrations of 10 µg/mL, 50 µg/mL, 100 µg/mL, 250 µg/mL and 500 µg/mL. 5ml of each test samples was mixed with 2ml of antidiabetic reagent (20 mM sodium phosphate buffer (pH 6.9), containing 6 mM sodium chloride). Further, test mixtures were incubated with and without α-Amylase (0.5 mg/mL) for about 10 min at 25 ºC followed by 1% starch solution was added to the reaction mixture and incubation was continued for 30 min at 25 ºC. To stop the enzymatic reaction the colouring agent dinitro-salicylic acid (DNS) was added to the mixture and incubated again for about 5 min in the water bath and were allowed to cool to room temperature. At last, distilled water was added to the test mixtures and absorbance was measured using a UV-Visible spectrophotometer at the range of 540 nm.

$$\text{α- Amylase inhibition \%} = \left[\frac{\text{Abs. Cont} - \text{Abs. Sam}}{\text{Abs.Cont}}\right] \times 100 \quad \ldots\ldots\ldots\ldots\ldots\ldots\ldots\ldots \text{(4)}$$

where, Abs. Cont and Abs. Sam are absorbance of control and absorbance of extract respectively.

2.9 Drug Loading

The ability to control drug loading and release play the most important role in the development of medical devices. The biological inspiration of biopolymer blended HA and MMT clay composites has been determined through the drug loading / releasing nature of the composites. The drug loading ability of synthesized fishbone polymer matrix was measured by UV–spectrophotometry method. Briefly drug was dissolved in methanol (5:1 w/v) and then solution was added drop wise to the 20 mg/ml of polymer composite in methanol with constant stirring using a magnetic stirrer at room temperature. After 24 hours, the prepared composite materials were separated out by centrifugation and the drug encapsulation efficiency can be evaluated by measuring the amount of unloaded drug in the supernatant solution at 425 nm (curcumin) and 480 nm (doxorubicin) using a UV-spectrophotometer **[30].** The experiments performed in triplicate. The encapsulation efficiency (%) of prepared composite was calculated using following equation

$$\text{Encapsulation efficiency (EE) \%= (Wt/ Wi) x 100} \quad \ldots\ldots\ldots\ldots\ldots\ldots\ldots\ldots \text{(5)}$$

where, Wt = amount of drug added – free non entrapped drug and Wi = total amount of drug.

2.10 Kinetic studies of *In-vitro* drug release

The drug release profile of drug-polymer matrix was investigated at different time and pH (5.5, 6.8 and 7.4) using phosphate buffer solution at room temperature. Dialysis tube technique was used to study the

in vitro drug release from prepared biocomposite.. The prepared biopolymer-drug material was subjected to a 12 kDa (Himedia, Dialysis membrane-110) dialysis membrane tube and it was dipped into a beaker containing 30 mL of Phosphate-buffered saline (PBS) buffer. At various time intervals, 1 mL of the supernatant was sample drawn and then 1ml of fresh PBS buffer was added into the release medium to maintain constant volume. The amount of the released drug was determined by measuring the absorbance of the sampled solution in the range of 425 nm (curcumin) and 480 nm (doxorubicin) using a spectrophotometer at different time intervals **[31]**.The drug release mechanism was determined by fitting experimental data with several drug release model such as Korsmeyer Peppas, Zero-order kinetics, First-order kinetics and Higuchi equation. The kinetics studies of drug release from biopolymer composite carrier measured using the following equations

Korsmeyer Peppas equation $\mathbf{F = (M_t / M_\infty) = Kt^n}$ **…… (6)**

where, M_t - accumulative amount of drug released at the time (t), M_∞- initial drug loading, K - constant for the drug-polymer system, and n is the diffusion exponent. According to Fickian theory, the profile of drug release includes zero-order kinetics, first-order kinetics and the Higuchi equation.

Zero-order kinetics $\mathbf{F_t = K_0 t}$ **…… (7)**

where, F – a fraction of drug release in time (t) and K_0- zero-order drug release constant.

First-order kinetics $\mathbf{\ln (1-F) = -K_1 t}$ **…… (8)**

where, F – a fraction of drug release in time (t) and K_1 – first-order drug release constant.

Higuchi equation $\mathbf{F = K_2 t^{1/2}}$, the equation that allowed for the quantification of drug release from a composite containing the finely dispersed drug **…… (9)**

Where, F – a fraction of drug release in time (t) and K_2 – Higuchi constant.

Results And Discussion

3.1 Fourier Transform Infra-red (FT-IR) Spectroscopy analysis

FT-IR spectra were studied for hydroxyapatite (HA), montmorillonite-hydroxyapatite (HA/MMT), sodium alginate-hydroxyapatite (HA/SA) and montmorillonite-sodium alginate-hydroxyapatite (HA/MMT/SA) polymer matrix. Fig.1 shows the spectra of the synthesized biopolymer derivatives. The FT-IR spectrum of Fish bone-hydroxy apatite (fig.1a) was observed as a broad peak at the range of 3411 cm^{-1} and 3213 cm^{-1} which indicates the presence of hydroxyl (-OH) group at phosphate molecule in the compound **[32]**. The peak at 1635 cm-1 was observed due to the stretching vibration of an adsorbed water molecule. This reveals the hydrophilic nature of fishbone-hydroxy apatite. The sharp infrared peaks at 1089 cm^{-1} and 827cm^{-1} were corresponding to asymmetric and symmetric stretching frequencies of phosphate

molecules respectively. Bending vibrations were observed in the range between 599 cm^{-1} and 557 cm^{-1} indicating the presence of a third phosphate molecule in the hydroxyapatite compound **[33, 34]**.

The FT-IR spectrum of the HA/MMT composite showed in fig.1b. The broad peak was found at 3631 cm^{-1} which indicates the structural –OH stretching frequency of MMT. Another broad peak was observed at 3378 cm^{-1} this could be the hydroxyl group of phosphate in HA **[35]**. A peak that appeared at 1634 cm^{-1}indicates the –OH bending vibration of a water molecule in the composite. The sharp peak at 1019 cm^{-1} reveals the presence of silicon-oxide (Si-O) conjugation at the clay. The aggregated peaks were observed at 600 cm^{-1} and 559 cm^{-1} and this was confirmed the presence of the O-P-O bond of HA **[36]**.

Fig.1c. shows the FT-IR spectrum of Hydroxyapatite-Sodium alginate (HA/SA). The IR bands appeared at 824 cm^{-1}, 462 cm^{-1}, 1019–1158 cm^{-1} and 557–599 cm^{-1}corresponds to wavenumbers ($\bar{\upsilon}_S$, δ_S, $\bar{\upsilon}_{aS}$ and δ_{aS}) of phosphate groups of the HA **[37]**. Another, two peaks were observed at 660and 1419 cm^{-1} due to the presence of hydrogen phosphate (HPO_4^{2-}) and carbonate (CO_3^{2-}) groups respectively. Moreover, due to the presence of hydroxyl ions were assigned the IR bands at 3274 cm^{-1} ($\bar{\upsilon}S$) and 557 cm^{-1} ($\bar{\upsilon}L$) respectively. This revealed the important characteristic peak of the Biopolymer composite **[38]**. The peaks at 2903 cm^{-1} and 1597 cm^{-1} were attributed to the presence of surface water in the hydroxyapatite. The interaction of hydroxyapatite onto Biopolymer (sodium alginate) modified the surface and this might decrease the intensity of hydroxyl (–OH) bands ($\bar{\upsilon}S$ and $\bar{\upsilon}L$) by adding sodium alginate. After the formation of composite, new vibrations bands appeared at 1597 cm^{-1}, 1333 cm^{-1} and 1419 cm^{-1} respectively which are attributed to the carboxyl (COO–) groups of SA. The peak observed at 824 cm^{-1} confirms the presence of triple vibrational modes ((τ (CO), δ (CCO), δ (CCH)) in the Ca-alginate. After the insertion of HA in SA, the band intensity was shifted 824 cm^{-1}. This wavenumber conversion indicates that the sodium alginate has not interacted with the P-OH active site of HPO_4^{2-} groups **[39]**.

The FT-IR spectrum analyzed for the HA/MMT/SA composite was shown in fig.1d. The hydrogen-hydrogen interaction on composite has been confirmed by the broad IR bands at 3623 cm^{-1} and 3213 cm^{-1} in the polymer which reveals that wavenumbers for hydroxyl of phosphate have been shifted in the IR region in the MMT clay and hydroxyapatite. The peaks were observed at 3070 cm^{-1} and 1598 cm^{-1} respectively which indicates the presence of water molecule interaction on the surface of the Biopolymer composite. The peaks at 1420 cm^{-1} and 1334 cm^{-1} correspond to the carboxyl group of the polymer Na-alginate. The IR spectrum of composite shows the characteristics peaks of glycosidic (C-O-C) linkage and absorption band of C-H deformation which corresponds to the vibration of β-pyranose at 1147-1011 cm^{-1} and 826 cm^{-1}, respectively. The IR bands have seen around 600 cm^{-1}, 556 $cm^{-1}$and 3521 cm^{-1} for HA/MMT/SA composite was attributed to the O-P-O bending of phosphate groups and stretching mode of –OH water present in the polymer matrix **[40]**. Another band shift was observed from 1634 cm^{-1} to 1597 cm^{-1} and 1598 cm^{-1} in HA/MMT and HA/MMT/SA composites respectively. This corresponds to –OH bending of a water molecule in MMT clay which further confirms the occurrence of different interactions such as electrostatic interactions and hydrogen bonding, of the Na-alginate with the MMT

clay and HA**[41]**. This supports the presence of MMT clay in the composites HA/MMT and HA/MMT/SA. The discussed wavenumbers for a functional group in the FT-IR spectra confirm the association of MMT and HA have been incorporated successfully in the Biopolymer composite.

3.2 X-ray Diffraction (XRD) studies

X-ray diffractogram of HA, HA/MMT, HA/SA and synthesized clay blended Biopolymer composites (HA/MMT/SA) were analysed using XRD as shown in fig.2.The XRD spectrum of the HA was shown in Fig.2a. The prominent characteristic peaks of HA were observed 2θ = 26.197°, 32.054° , 53.557° and 71.72° and the d space values of 2θ were found to be 3.44, 2.77, 1.722 and 1.316 respectively. Moreover, the observed values were in good agreement with the reference (ICDD-PDF# 09-0432) values of HA. Respective planes of 2θ values (002), (112), (004) and (431) show that the prepared HA has crystalline corresponding to Hydroxyapatite **[42]**. The X-ray diffraction peak of MMT at 2θ = 7º was not observed in the HA/MMT matrix, due to exfoliation. This shown as supportive document in S.fig.1 **[43]**. The new diffraction peak was observed at 2θ =19.76 (d space= 4.48, plane = 100) and 26.85, which shown in fig.2b confirmed the formation of a polymeric hybrid structure **[44]**. After the formation of polymer composite, the crystalline nature of hydroxyapatite was found to decrease due to the interaction of hydrogen atoms. This modification changes the crystallinity to the amorphous state, which had been confirmed through the formation of the aggregated peak from a sharp peak.

Fig.2c shows the XRD patterns of the HA/SA composite. A broad peak was found at 26.13° for the polymer sodium alginate, whereas a sharp peak was observed at 32.09° for hydroxyapatite **[45]**. Apparently, after the inclusion of sodium alginate, the shifting and decreasing in the crystallinity of major peaks of pure Hydroxyapatite, obviously indicates the presence of interaction between alginate and Hydroxyapatite.

Similarly, according to Zhang et al, the intensity of major characteristics peaks of HA/SA was found weak owing the composite was mainly composed through the cross-link reaction of SA on HA **[46]**. Probably, by adding SA in HA, the interaction between calcium cation (Ca^{2+}) of HA and carboxyl (COO^{-}) ion of alginate could increase the structural bridges in the Biopolymer composite **[47]**.The crystalline size of the prepared composite was given in S.Table.1 as a supportive document. This confirms the crystallinity of HA was affected after the formation of the composite.

The XRD pattern of Biopolymer hybrid (HA/MMT/SA) diffraction peaks was observed at 26.57º and 32.15º corresponds to HA and this confirmed the presence of HA in composite (fig.2d). Further, the peaks at 23.54º and 26.57º in HA/SA and HA/MMT/SA composite composites were revealed the presence of SA and MMT, respectively **[48]**. The obtained results concluded that the presence of phosphate (PO_4^{3-}) groups on the surface of the HA and enhancing the hybridisation of MMT and resulted in simultaneous interaction of MMT and HA with the carboxylic (COO^{-}) ions of sodium alginate. Thus, the X-ray diffractograms reveal that the interacting molecules of HA, MMT and SA have been successfully

incorporated each other in the Biopolymer hybrid composites. The obtained crystallite value of the prepared compounds reveals the order of amorphous nature of the composites which are shown below

HA/MMT/SA >> HA/SA >> HA/MMT >> HA

3.3 Thermogravimetric – Differential thermal (TGA-DTA) analysis

Thermal analysis of HA, HA/MMTand synthesized Biopolymer hybrid shown in fig.3. The thermal curves of HA were appeared at 81 °C and 230 °C as endothermic peaks, this could be due to the loss of physically absorbed water molecules and the elimination of water lattice in the compound **[49]**.The first mass loss of HA had about 5.40% at 127 °C and this mass loss existed between first and second endothermic peaks. The second mass loss had about 22.14% between 150 °C and 400 °C, this could be the dehydration of phosphate (HPO_4^{2-}) ions molecules due to calcination. The third mass loss had about 3.94% at 780°C due to the decomposition of HA into the whitlockite phase**[50]**. The thermal decomposition of HA has been extended due to the presence of calcium (Ca^{2+}) metal ions in the compound and it is shown in fig.3a.

The TGA-DTA curves of HA/MMT clay composite are shown in fig.3b.The mass loss of about 5.38% for HA/MMT composite occurred at the temperature of 95 °C due to the volatilization in the residual water (moisture) molecule and also the water molecules bound at the exchangeable cations in the interlayer space at the composite **[51]**. The second mass loss had about 5.89 % for composite between 400 °C and 600 °C due to the dehydroxylation of the structural water of the clay and the loss of water molecules associated with the phosphate groups in HA. The residual mass was found to be 88.71% for the composite, this could be the contribution of un-burnt metal (Na^+, K^+, Ca^{2+}, Fe^{2+}, Al^{3+}, Si^{4+}) ions in the composite, which extends the thermal stability of the composite more than 800 °C **[52]**.

The thermal degradation for HA/SA composite (fig.3c) had about 5.54 % at 120 °C, an endothermic peak was observed at 136 °C due to the removal of adsorbed surface water moisture in the Biopolymer composite. Additionally, the exothermic peak showed at 216 °C is corresponds to the breakdown of alginate chains in the hybrid composite, this confirms through the absence of an exothermic peak in the DTA curve of unblended HA (Fig.3a). Another thermal decomposition was observed between 200 °C and 400 °C with a weight loss of 29.47 %, because of the eruption of the carboxylic (COO^-) group, damage of glycosidic (C-O-C) linkage in the polymer and dehydroxylation of phosphate molecules in HA **[53]**.

Thermal curves of HA/MMT/SA of shown in fig.3d. The exothermic peak was observed in the DTA curve at 217 °C due to the thermal decomposition of the alginate chain in the composite. About 10 % thermal decomposition for the prepared compounds showed that HA/MMT had more thermal stability than starting material HA and the prepared composites, this might be the reason for non-combustible residual mass and metal ions in the polymer composite. The order of the thermal stability of the prepared compounds were shown below.

HA/MMT >> HA >> HA/SA >> HA/MMT/SA

3.4 Field emission-scanning electron microscope (FE-SEM) analysis

The surface morphology of HA and synthesized composite (HA/MMT, HA/SA and HA/MMT/SA) were shown in fig.4. Figure 4a shows the morphological surface of HA, which shows irregular particles, with a strong tendency for aggregation. The image showed that particles have been hugely agglomerated in the compound due to the particle-particle interaction of hydroxyapatite **[54]**. This is further confirmed through a spectrum of EDAX (Ca, P, and O peaks of HA are available) as shown in Fig. 5a. Certainly, the HA is utilized in hard tissue repairing due to structural and chemical properties of hydroxyapatite similar to the mineral phase of bone.

The prepared HA/MMT composite composites appeared as porous, the size of pores at 100 nm which is shown in fig.4b. Figure 4a showed that the size of the pore has a wide range of distribution ranging in the composite. After the addition of MMT in HA, the size of the pore and the density were found to decrease. This clearly evident the microstructures of HA that the inclusion of MMT had reduced the pore sizes of composite composites (HA/MMT) as compared to pure HA. The absence of agglomeration in the prepared composite indicates that MMT clay particles have been distributed uniformly in the HA compound **[55]**. The change in the morphological surface of HA confirms the formation of the composite.

Similarly, SEM images of HA/SA possess a wide range of porous structures which are shown in fig.4c. The composite prepared in the presence of SA, become agglomerates in their shapes with different sizes and poorly defined shapes. The HA/SA composite appeared as a whitlockite phase after incorporation of biopolymer SA in hydroxyapatite **[56]**. The modification occurred in the structure due to particle-by-particle interaction and the electrostatic interaction between HA and SA in the composite. The successful association of composite has more preferable to the alteration that occurred in the morphological surface of blended HA on SA. The Biopolymer blended HA/MMT composite microstructure is shown in fig.4d.

The microstructures of HA were affected due to a decrease in the porous size of particles in the composite composites (HA/MMT/SA) after the addition of MMT and SA in hydroxyapatite respectively. Additionally, SEM micrographs revealed that the composite became homogeneous and rugged after insertion of both MMT and SA particles in the HA and there was also no evidence of agglomeration **[57]**. This might be the interaction between carboxylic (COO^-) and hydroxyl (OH^-) group of the SA, and the phosphate and Ca^{2+} ion of the HA. The physical properties of composite such as rogocity nature, uniformity and firmly assimilation of pathogens are supports for the composite to reveal various biological applications such as antimicrobial, antioxidant, antidiabetic, anti-inflammatory, hemolysis and drug release.

3.5 Energy dispersive spectroscopic (EDAX) analysis

The EDAX spectra of HA incorporated derivatives have confirmed the presence of constituents and weight percentage of C, O and metal ions. The EDAX spectrum of HA displays weight percentages of carbon, oxygen, phosphorous and respective metal (Ca^{2+}) ion corresponds for the formed calcium hydroxyapatite

(HA) which is shown in fig.5a. Figure 5b showed the EDAX spectrum of the matrix MMT clay blended HA **[58]**.

The obtained EDAX spectrum showed decrease in the percentage of calcium and phosphorous and additionally the composite had been possessed silicon ion which confirmed the presence of MMT in the polymer hybrid. Energy dispersive peaks of HA/SA composite showed in fig.5c. The peak intensities (cps/eV) were observed with the weight percentage such as carbon-4.5%, oxygen-9.75%, phosphorous-1.19% and calcium-2.08%. This clearly reveals that the percentage of carbon has been increased due to the presence of sodium alginate in a polymer matrix. Similarly, the EDAX peaks for HA/MMT/SA (fig.5d) were obtained such as carbon, oxygen, silicon, phosphorous and calcium metal ions were found in the spectrum. The presence of peak for silicon in the spectrum that strongly evident the presence of MMT clay in the composite, the presence of calcium and phosphorous corresponds to the presence of HA in the composite **[59]**. Moreover, the increase in the percentage of carbon (5.52%) indicates the presence of sodium alginate in the hybrid. The EDAX spectra of the HA derivatives showed strong evidence of the successfully formed composite. The obtained elements weight percentage values were given as supportive documents in S.Table.2.

3.6 Ultra Violet– Visible spectral analysis

The UV-Vis diffuse reflectance spectra of pure HA derivatives show a redshift of the absorption edges for the composite systems compared to pure hydroxyapatite (HA). The pure HA absorbs only the UV light of less than 350 nm which shows significant contraction than the composites in the UV-Visible region. The extent of redshift depending on the metal ions present in the composite was absorbed in visible light, which has been not exceeded more than 550 nm **[60]**. The prepared composites showed redshift and strong absorption in both visible and UV–Vis light regions which may enhance the photocatalytic activities in the dye degradation.

3.7 Porosity studies

The prepared HA using fishbone and their derivatives HA/MMT, HA/SA and HA/MMT/SA were studied for the porosity percentage. The obtained porosity percentage of the compound was compared with the biological studies i.e. the increase in the porosity of the compound showed more activity in biological applications such as antimicrobial, antioxidant, antidiabetic and drug-releasing studies **[60]**.This may be due to the excessive reactive oxygen species (ROS) formation at the homogeneous and porous surface of substances that might be preferable to induce oxidative stresses leading to cell damage and cell death. The order of porosity percentage for prepared HA derivatives was shown below and the porosity percentage has been given as supportive information in S.Table.3.

HA/MMT/SA >HA/MMT >HA/SA > HA

3.8 Antibacterial activity

The antibacterial studies were carried out for the prepared HA, HA/MMT, HA/SA and HA/MMT/SA compounds. The antibacterial potential of the composite was evaluated according to their zone inhibition method. The antibacterial results showed scavenging more in the bacterial zone for the Biopolymer blended MMT and HA composite. There is no change was occurred in the zones of inhibition around the negative control wells on agar **[61]**. A correlation was observed between the size of inhibition in the zone and concentration of compound i.e. when the diameter of the inhibitory zone increased with increased concentration of compounds. The composite affects more in the bacterial zone of *S.aureus* and *P.aeruginosa* and thereby this confirms the composite HA/MMT/SA had more bacteriostatic action than other prepared compounds in the bacterial zone. The minimum and maximum concentrations of prepared test samples and their activity against bacteria were shown in fig.6. The maximum inhibition for 250 µL concentration of HA/MMT/SA has affricate well up to 34 mm against the *S.aureus* bacterial zone **[62]**. The prepared Biopolymer composite showed significantly antagonistic against all the bacteria and better results than standard drug ampicillin. The increasing order of affected bacterial growth through the prepared HA and their composite derivatives were shown below.

S.aureus > B. Subtilis>E.coli > P.aeruginosa

3.9 Total antioxidant efficacies

The naturally forming free radicals are highly unstable molecules in the human cells, when doing works food converts into energy. Hence, anti-oxidant substances have been used to prevent cell damage in the human cell. The enzymatic and non-enzymatic reaction affects the cells in the human for free radical formation, which leads to occur continuously. The total antioxidant studies showed that the composites exhibit better antioxidant results. The results of percentage inhibition of free radical activity were shown in fig. 7. The obtained free radical inhibition results of prepared composites were compared with the standard drug vitamin C **[63]**. The antioxidant results for the maximum concentration of the compound (HA/MMT/SA) showed 78.48 ± 2.5 % and the vitamin C was exhibited 83.89 ± 2.7 %. The order of percentage inhibition of free radical was shown in below

Vitamin C > HA / MMT / SA > HA / MMT > HA / SA > HA

3.10 Drug loading and release studies

With enhancing the addition of MMT clay and SA in the HA, drug loading percentage was increased due to hydrogen bonding between the carboxylic group of SA, hydroxyl groups of MMT and the amine of doxorubicin and OH^- group of curcumin (Fig. 8). Cumulative drug release rate decreased when compared with drug loading content, this might be related to ionic strength and the more cross-linking agent involvement during the reaction. The variation in the rates and amounts of the drug-releasing ability of drugs could be due to swelling behavior and interaction within the drug-polymer matrix **[64]**.

Curcumin comprising polyphenolic compounds had been extracted from turmeric. Over past decades, many reports have been coming on the work of pharmacological activities like anti-cancer, anti-alzheimer,

anti-diabetic, anti-bacterial, anti-inflammatory and so on. About 79.83 % of curcumin drug loaded in the prepared HA/MMT/SA composite had been measured using a UV (Shimadzu UV 3600) spectrophotometric method. In this drug loading and delivery study, the curcumin showed better releases from Biopolymer material than reported studies i.e. for the prepared Biopolymer composite HA/MMT/SA releases 70.12 % of curcumin to the target. At pH = 5.5, the curcumin drug-releasing results shows 70.12 %, at pH = 6.8 shows 50.85 % and at pH = 7.4 shows 34.91 %. The change in the drug-releasing ability of curcumin at various pH (5.5, 6.8 and 7.4) is due to the functional group of curcumin that exists in the molecule **[65]**. Cancer producing cells replicate at pH = 5.5, thus the curcumin, enhancing the releasing rate at pH = 5.5 which is shown in fig.8a. This proves the prepared Biopolymer composite might be the better drug-releasing candidate for cancer treatment.

Doxorubicin (DOX) widely employed in chemotherapy treatment, is the most effective chemotherapeutic drug developed against cancer cells such as solid tumors, transplantable leukemia, lymphomas and etc. The doxorubicin drug loaded in the prepared HA/MMT/SA composite had loaded more than curcumin and the drug has been loaded 90.78%. The percentage of drug encapsulation has been more when compared to the drug releases because of the interactions of hydrogen – hydrogen between the OH- group of DOX and the OH- group of polymer hybrid i.e. the drug DOX has been released to the target about 81.18 % which is shown in fig. 8b. At pH = 5.5, the doxorubicin drug-releasing results shows 81.18 %, at pH = 6.8 shows 58.06 % and at pH=7.4 shows 35.08 % **[66]**.

The change in the drug-releasing ability of doxorubicin at various pH (5.5, 6.8 and 7.4) is due to the functional group of doxorubicin that exists in the molecule. The functional groups on the polymer matrix of HA/MMT/SA enhanced the loading efficiency by the stronger interaction with MMT and SA. Various drug delivery systems are widely in the field of pharmaceutical and biomedical applications. The residual free -COOH groups and OH- in the Biopolymer composite, protonated at acidic pH (5.5), further confirms through the swelling thereby producing greater repulsive force. The obtained results showed better drug release properties for prepared HA/MMT/SA composite than reported compounds. This is shown in S.Table.4 as supportive information.

3.10 Kinetic studies of *In-vitro* drug release

The drug release profiles of curcumin from HA/MMT/SA Biopolymer composite composites carried out at different pH (5.5, 6.8 and 7.4) at 37 ºC were graphically represented in fig 8a**.** These three pH values were selected because the drugs might be exposed to those pH conditions while moving through the blood to liver cancer cells. The hybrid composite HA/MMT/SA had more release quantity at pH=5.5, compared to the pH=6.8 and pH=7.4, this hybrid composite HA/MMT/SA had the better-sustained release of curcumin for over 32 hrs. These results were obtained due to the participation of numerous -OH and -NH groups between HA/MMT and SA in the composite. The obtained result shows that the release rate in pH=5.5 was higher than pH=6.8 and 7.4.The solubility shows higher for both doxorubicin and curcumin due to lower pH, which helps to intake the drug for release to the cells or to the solid tumours, from the HA/MMT/SA incorporated drugs or biomolecules **[67]**. The decrease occurs in the curcumin drug release

due a lower solubility at basic pH (6.8 and 7.4). At lower pH (acidic), the basic (-NH_2) centre of curcumin enhances the neutral nature, which has helped to increases the solubility of curcumin.

Similarly, the drug release reports of doxorubicin from HA/MMT/SA Biopolymer composite composites were studied at different pH (5.5, 6.8 and 7.4) at 37 ºC and were graphically represented in fig 8b**.** HA/MMT/SA composite had a better drug release amount at acidic pH=5.5 compare to the basic pH=6.8 and pH=7.4 and this Biopolymer hybrid composite HA/MMT/SA released the drug doxorubicin about 76.6 % in 32 hrs. These dramatic changes in the drug-releasing rates might be attributed to the contribution of the hydroxyl group and amine group at the drug, which reduces the drug release rate at basic pH (6.8, 7.4) due to the incorporation between the composite HA/MMT/SA. At lower pH (acidic) increases the solubility of doxorubicin due to the presence of a basic medium of drug and improves the neutral nature **[68]**. According to kinetic models such as zero-order, first-order, Higuchi and Korsmeyer-Peppas models, the kinetic parameters for both drugs released from the Biopolymer composites were analyzed.

A selecting criterion was the most suitable model R^2 close to unity. At selected all pH the correlation coefficient value (R^2) of the Higuchi model was greater than zero-order and the first-order model. The kinetic drug releases for doxorubicin show a value close to R^2=0.9939, which fits the Higuchi model. The R^2 values of the Higuchi model for the prepared composites were showed more linearity which indicated that the kinetics drug release of the drugs follows the diffusion-controlled method. The doxorubicin release mechanism was studied using the Korsmeyer-Peppas model. The diffusion exponent values obtained for the composite determine through the Korsmeyer-Peppas model found in the range of 0.5155 to 0.7829 at pH 5.5 indicates that diffusion is anomalous or non-Fickian. .

Similarly, the diffusion exponent values were obtained in the range of 0.3483 to 0.4988 at pH 6.8 and 0.1839 to 0.3385 at pH 7.4 respectively for the composites which indicates the drug follows Fickian diffusion behavior with controlled release by diffusion. The kinetic constant (k) value increase when composite content increases, suggesting the diffusion rate increases due to an increase in the size of free spaces in the composite network. The kinetic drug releasing values of curcumin and doxorubicin are given in S.Table.5a and S.Table.5b as supportive information.

At pH=5.5, the curcumin diffusion exponent value for composites showed the ranges between 0.3889 and 0.4901, drug follows Fickian diffusion and the composite HA/MMT/SA shows the value 0.6016, indicates coupling of diffusion and matrix erosion mechanism. At pH=6.8 the composite shows the range between 0.1089 and 0.2509, drugs follow Fickian diffusion. At pH=7.4 the composite shows the range from 0.1134 to 0.2802, indicates that the drug follows Fickian diffusion **[69]**. In general, drug release from a polymeric matrix is described by a fickian mechanism when drug diffusion is the main factor in drug release. Diffusion of the drug from a polymeric composite can occur through drug diffusion out of composite. Non-fickian behavior was also found in all pH values (5.5, 6.8 and 7.4). This indicates that diffusion and relaxation of polymer is involved in the drug-release mechanism.

3.11 Antidiabetic assay (α-amylase inhibition method)

The plot of α-amylase inhibition was evaluated in terms of percentage for prepared Biopolymer composites as shown in fig.9. In this analysis, significant differences were found between HA and inserted clay / Biopolymer. Antidiabetic drugs used in diabetes treat diabetes mellitus by altering the glucose level in the blood. These α- amylase inhibitors or starch blocker prevents or slows the absorption of sugar content into the body, mainly blocks the formation oligosaccharides into monosaccharides such as glucose, fructose, maltose etc. through hydrolysis of 1,4-glycosidic (C-O-C) linkages of starch **[70]**.

The obtained α-amylase inhibition results of prepared composites were compared with the standard drug acarbose. The antidiabetic results for the maximum concentration of the compound (HA/MMT/SA) showed 83.96 ± 1.5 % and the acarbose was exhibited 80.82 ± 1.6 %. The obtained results of the prepared Biopolymer hybrid composite reveals that the composite had more antidiabetic properties than acarbose this might be preferable to utilize as a better antidiabetic drug in the biomedical field. The order of percentage inhibition of α-amylase for the prepared HA, HA/MMT, HA/SA, HA/MMT/SA and the standard drug acarbose were shown below.

HA/MMT/SA >> Acarbose >> HA/MMT >> HA/SA >> HA

Conclusion

The prepared Biopolymer composite HA/MMT/SA was successfully coordinated through the co-precipitation method. The FT-IR and XRD results confirmed the formation of composites. The presence of metal ions in the clay blended Biopolymer derivatives was extended the thermal stability of the composites, this further confirmed through EDAX spectra of the composites. After the incorporation of MMT clay and Biopolymer sodium alginate on HA, the morphological surface image was changed. The increases in the porosity of the composite showed better biological activities of the prepared polymer composites. *S.aureus* bacterial growth had more infected by the prepared composites, the maximum inhibition of HA/MMT/SA have affricate well up to 34 mm against the *S.aureus* bacterial zone. The antioxidant results for the maximum concentration of the compound (HA/MMT/SA) showed 78.48 ± 2.5% and the vitamin C was exhibited 83.89 ± 2.7%. Doxorubicin and curcumin drug release was investigated at different pH mediums and reports that the drug release was strong pH dependence. The results revealed that doxorubicin and curcumin loaded composite has a significant enhancement in drug release ability as compared to pure hydroxyapatite. Drug release showed higher at pH 5.5 compared to the pH 6.8 and 7.4, it has been noticed that the prepared composite reveals a better candidate for modified / controlled drug delivery. The composite showed slow and continuous release during kinetic in-vitro drug controlled release studies and sustained drug release was noticed with non-fickian diffusion and relaxation of polymer mechanism in the kinetic drug release studies. Therefore, the prepared composites consisting controlled drug delivery system is preferable to releases the drug as therapeutic agents in a specific target as needed to achieve the desired therapeutic outcome.

Declarations

Acknowledgment

The authors thanks to Department of chemistry, Anna University to facilitated and provided the sophisticated laboratory besides Dr. M. Manimohan, PG and Research department of chemistry, Islamiah College (Autonomous), Vaniyambadi to carry this research work. Also thank to the management of Islamiah College (Autonomous), Vaniyambadi, Tamilnadu, India.

References

1. H. Ma, C. Feng, J. Chang, C. Wu, 3D-printed bioceramic composites: From bone tissue engineering to tumor therapy. Acta Biomater. **79**, 37–59 (2018). doi:10.1016/j.actbio.2018.08.026
2. E. Sharifisamani, F. Mousazadegan, R. Bagherzadeh, M. Latifi, PEG-PLA-PCL based electrospun yarns with curcumin control release property as suture. Polym. Eng. Sci. **60**(7), 1520–1529 (2020). doi:10.1002/pen.25398
3. S. Lawson, K. Newport, N. Pederniera, A.A. Rownaghi, F. Rezaei, Curcumin Delivery on Metal–Organic Frameworks: The Effect of the Metal Center on Pharmacokinetics within the M-MOF-74 Family. ACS Appl. Bio Mater. **4**(4), 3423–3432 (2021). doi:10.1021/acsabm.1c00009
4. C. Chen, L. Lu, S. Yan, H. Yi, H. Yao, D. Wu, X. Deng (2018). Autophagy and doxorubicin resistance in cancer. Anti-Cancer Drugs, 29(1), 1–9. doi:10.1097/CAD.00000000 00000572
5. J. Li, M. Liu, Y. Qiu, Y. Gan, H. Jiang, B. Liu, N. Ma, Urchin-like Hydroxy apatite/Graphene Hollow Microspheres as pH-Responsive Bone Drug Carriers. Langmuir **37**(14), 4137–4146 (2021). doi:10.1021/acs.langmuir.0c03640
6. C. Tian, P. Xu, J. Jiang, C. Han (2021). Preparation and drug-delivery study of functionalized hydroxyapatite based on natural polysaccharide gums with excellent drug-loading properties. Journal of Dispersion Science and Technology, 42(5), 751–759. doi: 10.1080/01932691.2019.1710185.
7. Wang, M. Li, M. Wang, Y. Shao, Y. Zhu, Y., & S. Yang (2021). Efficient antibacterial activity of hydroxyapatite through ROS generation motivated by trace Mn (iii) coupled H vacancies. Journal of Materials Chemistry B, 9(15), 3401–3411. doi:10.1039/D1TB00098E
8. S. Mondal, G. Hoang, P. Manivasagan, M.S. Moorthy, T.T.V. Phan, H.H. Kim, J. Oh, Rapid microwave-assisted synthesis of gold loaded hydroxyapatite collagen nano-bio materials for drug delivery and tissue engineering application. Ceram. Int. **45**(3), 2977–2988 (2019). doi:10.1016/j.ceramint.2018.10.016
9. N.L. Fernando, D.T. Rathnayake, N. Kottegoda, J.S. Jayanetti, V. Karunaratne, D.R. Jayasundara, Mechanistic Insights into Interactions at Urea–Hydroxyapatite Nanoparticle Interface. Langmuir **37**(22), 6691–6701 (2021). doi:10.1021/acs.langmuir.1c00564
10. M. Irfan, P.S. Suprajaa, R. Praveen, B.M. Reddy, Microwave-assisted one-step synthesis of nanohydroxyapetite from fish bones and mussel shells. Mater. Lett. **282**, 128685 (2021). doi:10.1016/j.matlet.2020.128685

11. C.M. Mardziah, S. Ramesh, C.Y. Tan, H. Chandran, A. Sidhu, S. Krishnasamy, J. Purbolaksono, Zinc-substituted hydroxyapatite produced from calcium precursor derived from eggshells. Ceram. Int. **47**(23), 33010–33019 (2021). doi:10.1016/j.ceramint.2021.08.201
12. A. Pal, S. Paul, A.R. Choudhury, V.K. Balla, M. Das, A. Sinha, Synthesis of hydroxyapatite from Lates calcarifer fish bone for biomedical applications. Mater. Lett. **203**, 89–92 (2017). doi:10.1016/j.matlet.2017.05.103
13. H.B. Modolon, J. Inocente, A.M. Bernardin, O.R.K. Montedo, S. Arcaro (2021). Nanostructured biological hydroxyapatite from Tilapia bone: a pathway to control crystallite size and crystallinity. Ceram. Int., 47(19), 27685–27693. doi:10.1016/j.ceramint. 2021.06.193
14. N. Fijoł, H.N. Abdelhamid, B. Pillai, S.A. Hall, N. Thomas, A.P. Mathew, 3D-printed monolithic biofilters based on a polylactic acid (PLA)–hydroxyapatite (HAp) composite for heavy metal removal from an aqueous medium. RSC Adv. **11**(51), 32408–32418 (2021). doi:10.1039/D1RA05202K
15. B.R. Sunil, M. Jagannatham, Producing hydroxyapatite from fish bones by heat treatment. Mater. Lett. **185**, 411–414 (2016). doi:10.1016/j.matlet.2016.09.039
16. T. Maschmeyer, R. Luque, M. Selva, Upgrading of marine (fish and crustaceans) biowaste for high added-value molecules and bio (nano)-materials. Chem. Soc. Rev. **49**(13), 4527–4563 (2020). doi:10.1039/C9CS00653B
17. S. Mondal, U. Pal, 3D hydroxyapatite composite for bone regeneration and local drug delivery applications. J. Drug Deliv. Sci. Technol. **53**, 101131 (2019). doi:10.1016/j.jddst.2019.101131
18. Z. Mahcene, A. Khelil, S. Hasni, P.K. Akman, F. Bozkurt, K. Birech, F. Tornuk, Development and characterization of sodium alginate based active edible films incorporated with essential oils of some medicinal plants. Int. J. Biol. Macromol. **145**, 124–132 (2020). doi:10.1016/j.ijbiomac.2019.12.093
19. M. Xu, M. Qin, Y. Cheng, X. Niu, J. Kong, X. Zhang, H. Wang, Alginate microgels as delivery vehicles for cell-based therapies in tissue engineering and regenerative medicine. Carbohydr. Polym. **266**, 118128 (2021). doi:10.1016/j.carbpol.2021.118128
20. F. Liu, X. Liu, F. Chen, Q. Fu, Mussel-inspired chemistry: A promising strategy for natural polysaccharides in biomedical applications. Prog. Polym. Sci. **123**, 101472 (2021). doi:10.1016/j.progpolymsci.2021.101472
21. N.F.A. Kasim, W.F.W. Idris, A.H. Abdullah, K. Yusoh, Z. Ismail, The preparation of graphene ink from the exfoliation of graphite in pullulan, chitosan and alginate for strain-sensitive paper. Int. J. Biol. Macromol. **153**, 1211–1219 (2020). doi:10.1016/j.ijbiomac.2019.10.251
22. Jariya, S. I., Padmanabhan, V. P., Kulandaivelu, R., Prakash, N., Mohammad, F., Al-Lohedan,H. A., … Sagadevan, S. (2021). Drug delivery and antimicrobial studies of chitosan-alginate based hydroxyapatite biocomposites formed by the Casein micelle assisted synthesis.Materials Chemistry and Physics, 272, 125019. doi: 10.1016/j.matchemphys.2021.125019
23. L. Mdlalose, M. Balogun, K. Setshedi, L. Chimuka, A. Chetty, Performance evaluation of polypyrrole–montmorillonite clay composite as a re-usable adsorbent for Cr (VI) remediation. Polym. Bull. **78**(8),

4685–4697 (2021). doi:10.1007/s00289-020-03338-6

24. S. Song, C. Zhang, J. Wang, W. Li, Z. Jiang, Y. Zhang, High-performance nacre-like graphene@ polymer supported montmorillonite composite actuator and sensor. Sens. Actuators B **332**, 129446 (2021). doi:10.1016/j.snb.2021.129446
25. L.H. de Oliveira, P. Trigueiro, J.S.N. Souza, M.S. de Carvalho, J.A. Osajima, E.C. da Silva-Filho, M.G. Fonseca, Montmorillonite with essential oils as antimicrobial agents, packaging, repellents, and insecticides: an overview. Colloids Surf., B **209**, 112186 (2022). doi:10.1016/j.colsurfb.2021.112186
26. M. Manimohan, S. Pugalmani, M.A. Sithique, Biologically active novel N, N, O donor tridentate water soluble hydrazide based O-carboxymethyl chitosan Schiff base Cu (II) metal complexes: Synthesis and characterisation. Int. J. Biol. Macromol. **136**, 738–754 (2019). doi:10.1016/j.ijbiomac.2019.06.115
27. M. Manimohan, R. Paulpandiyan, S. Pugalmani, M.A. Sithique, Biologically active Co (II), Cu (II), Zn (II) centered water soluble novel isoniazid grafted O-carboxymethyl chitosan Schiff base ligand metal complexes: Synthesis, spectral characterisation and DNA nuclease activity. Int. J. Biol. Macromol. **163**, 801–816 (2020). doi:10.1016/j.ijbiomac.2020.06.278
28. P. Kasangana, P. Haddad, T. Stevanovic, Study of Polyphenol Content and Antioxidant Capacity of Myrianthus Arboreus (Cecropiaceae) Root Bark Extracts. Antioxidants **4**(2), 410–426 (2015). doi:10.3390/antiox4020410
29. M. Manimohan, S. Pugalmani, M.A. Sithique, Biologically Active Water Soluble Novel Biopolymer/Hydrazide Based O-Carboxymethyl Chitosan Schiff Bases: Synthesis and Characterisation. J. Inorg. Organomet. Polym Mater. **30**, 3658–3676 (2020). doi:10.1007/s10904-020-01487-9
30. K. Jyoti, R.S. Pandey, P. Kush, D. Kaushik, U.K. Jain, J. Madan, Inhalable bioresponsive chitosan microspheres of doxorubicin and soluble curcumin augmented drug delivery in lung cancer cells. Int. J. Biol. Macromol. **98**, 50–58 (2017). doi:10.1016/j.ijbiomac.2017.01.109
31. Almeida, E. A. M. S., Bellettini, I. C., Garcia, F. P., Farinacio, M. T., Nakamura, C. V., Rubira, A. F., … Muniz, E. C. (2017). Curcumin-loaded dual pH- and thermo-responsive magnetic microcarriers based on pectin maleate for drug delivery. Carbohydrate Polymers, 171, 259–266. doi:10.1016/j.carbpol.2017.05.034.
32. E.M. Mahmoud, M. Sayed, A.M. El-Kady, H. Elsayed, S.M. Naga, In vitro and in vivo study of naturally derived alginate/hydroxyapatite bio composite composites. Int. J. Biol. Macromol. **165**, 1346–1360 (2020). doi:10.1016/j.ijbiomac.2020.10.014
33. C.Y. Beh, E.M. Cheng, N.F. MohdNasir, S.K. Eng, M.S. Abdul Majid, M.J.M. Ridzuan, S.F. Khor, N.S. Khalid, Dielectric and material analysis on physicochemical activity of porous hydroxyapatite/cornstarch composites. Int. J. Biol. Macromol. **166**, 1543–1553 (2020). doi:10.1016/j.ijbiomac.2020.11.034
34. J. Chakravarty, M.F. Rabbi, V. Chalivendra, T. Ferreira, C.J. Brigham, Mechanical and biological properties of chitin/polylactide (PLA)/hydroxyapatite (HAP) composites cast using ionic liquid

solutions. Int. J. Biol. Macromol. **151**, 1213–1223 (2019). doi:10.1016/j.ijbiomac.2019.10.168

35. Fernando, M. S., Wimalasiri, A. K. D. V. K., Ratnayake, S. P., Jayasinghe, J. M. A. R. B., William, G. R., Dissanayake, D. P., … de Silva, R. M. (2019). Improved nanocomposite of montmorillonite and hydroxyapatite for defluoridation of water. RSC Advances, 9(61), 35588–35598. doi:10.1039/c9ra03981c.
36. R. Nawang, M. Zobir Hussein, K. Amin Matori, A.C. Abdullah, C., & M. Hashim (2019). Physicochemical properties of hydroxyapatite/montmorillonite nanocomposite prepared by powder sintering. Results in Physics, 102540. doi:10.1016/j.rinp.2019.102540
37. Y. Guesmi, H. Agougui, R. Lafi, M. Jabli, A. Hafiane (2018). Synthesis of hydroxyapatite-sodium alginate via a co-precipitation technique for efficient adsorption of Methylene Blue dye. J. Mol. Liq., 249, 912–920. doi:10.1016/j.molliq.2017. 11.113
38. B.S. Gholizadeh, F. Buazar, S.M. Hosseini, S.M. Mousavi, Enhanced antibacterial activity, mechanical and physical properties of alginate/hydroxyapatite bionanocomposite film. Int. J. Biol. Macromol. **116**, 786–792 (2018). doi:10.1016/j.ijbiomac.2018.05.104
39. L. Ma, W. Su, Y. Ran, X. Ma, Z. Yi, G. Chen, X. Li, Synthesis and characterization of injectable self-healing hydrogels based on oxidized alginate-hybrid-hydroxyapatite nanoparticles and carboxymethyl chitosan. Int. J. Biol. Macromol. **165**, 1164–1174 (2020). doi:10.1016/j.ijbiomac.2020.10.004
40. S. Kar, T. Kaur, A. Thirugnanam, Microwave-assisted synthesis of porous chitosan–modified montmorillonite–hydroxyapatite composite composites. Int. J. Biol. Macromol. **82**, 628–636 (2016). doi:10.1016/j.ijbiomac.2015.10.060
41. A. Olad, F. Farshi Azhar, The synergetic effect of bioactive ceramic and nanoclay on the properties of chitosan–gelatin/nanohydroxyapatite–montmorillonite composite for bone tissue engineering. Ceram. Int. **40**(7), 10061–10072 (2014). doi:10.1016/j.ceramint.2014.04.010
42. Z. Chen, J. Zhai, D. Wang, C. Chen, Bioactivity of hydroxyapatite/wollastonite composite films deposited by pulsed laser. Ceram. Int. **44**(9), 10204–10209 (2018). doi:10.1016/j.ceramint.2018.03.013
43. T. Chen, Y. Yuan, Y. Zhao, F. Rao, S. Song, Preparation of montmorillonite nanosheets through freezing/thawing and ultrasonic exfoliation. Langmuir **35**(6), 2368–2374 (2019). doi:10.1021/acs.langmuir.8b04171
44. M. Sandomierski, Z. Buchwald, A. Voelkel, Calcium montmorillonite and montmorillonite with hydroxyapatite layer as fillers in dental composites with remineralizing potential. Appl. Clay Sci. **198**, 105822 (2020). doi:10.1016/j.clay.2020.105822
45. H. Luo, G. Zuo, G. Xiong, C. Li, C. Wu, Y. Wan (2016). Porous nanoplate-like hydroxyapatite–sodium alginate nanocomposite composites for potential bone tissue engineering. Materials Technology, 32(2), 78–84. doi:10.1080/10667857.2015.1125045.
46. X. Zhang, C. Huang, Y. Zhao, X. Jin (2017). Preparation and characterization of nanoparticle reinforced alginate fibers with high porosity for potential wound dressing application. RSC Advances,

7(62), 39349–39358. doi:10.1039/c7ra06103j

47. Y. Bi, Z. Lin, S. Deng, Fabrication and characterization of hydroxyapatite/sodium alginate/chitosan composite microspheres for drug delivery and bone tissue engineering. Mater. Sci. Engineering: C **100**, 576–583 (2019). doi:10.1016/j.msec.2019.03.040
48. V. Vyas, T. Kaur, A. Thirugnanam, Chitosan composite three dimensional macrospheric composites for bone tissue engineering. Int. J. Biol. Macromol. **104**, 1946–1954 (2017). doi:10.1016/j.ijbiomac.2017.04.055
49. M. Othmani, A. Aissa, A. Grelard, R.K. Das, R. Oda, M. Debbabi (2016). Synthesis and characterization of hydroxyapatite-based nanocomposites by the functionalization of hydroxyapatite nanoparticles with phosphonic acids. Colloids Surf., A, 508, 336–344. doi:10.1016/j.colsurfa. 2016.08.078
50. M.R. Senra, R.B. de Lima, D. Souza, de H.S., Marques, M. de F. V., & S.N. Monteiro, Thermal characterization of hydroxyapatite or carbonated hydroxyapatite hybrid composites with distinguished collagens for bone graft. J. Mater. Res. Technol. **9**(4), 7190–7200 (2020). doi:10.1016/j.jmrt.2020.04.089
51. **Laabd, M., Brahmi, Y., El Ibrahimi, B., Hsini, A., Toufik, E., Abdellaoui, Y., … Albourine,A. (2021). A novel mesoporous Hydroxyapatite@ Montmorillonite hybrid composite for high-performance removal of emerging Ciprofloxacin antibiotic from water: Integrated experimental and Monte Carlo computational assessment. Journal of Molecular Liquids, 338, 116705.doi:10.1016/j.molliq.2021.116705**
52. M. Joudi, H. Nasserlah, H. Hafdi, J. Mouldar, B. Hatimi, M.A.E. Mhammedi, &Bakasse, M. (2020). Synthesis of an efficient hydroxyapatite–chitosan–montmorillonite thin film for the adsorption of anionic and cationic dyes: adsorption isotherm, kinetic and thermodynamic study. SN Appl. Sci., 2(6). **doi**:10.1007/s42452-020-2848-3
53. Y. You, Z. KeqiQu, Huang, R. Ma, C. Shi, X. Li, Z. Guo, Sodium alginate templated hydroxyapatite/calcium silicate composite adsorbents for efficient dye removal from polluted water. Int. J. Biol. Macromol. **141**, 1035–1043 (2019). 10.1016/j.ijbiomac.2019.09.082. () .,. **doi**
54. M. Sabir, A. Ali, U. Siddiqui, N. Muhammad, A.S. Khan, F. Sharif, I. Ur Rehman (2020). Synthesis and characterization of cellulose/hydroxyapatite based dental restorative composites. J. Biomater. Sci. Polym. Ed., 1–10. doi:10.1080/09205063.2020.1777827
55. L. Pazourková, P. Peikertová, M. Hundáková, G. SimhaMartynková (2020). Preparation of calcium deficient hydroxyapatite on the montmorillonite substrate: Structure and morphology, Materials Today: Proceedings, 37, 35–41. doi:10.1016/j.matpr.2020.02.927
56. N. Kanasan, S. Adzila, N. AzimahMustaffa, P. Gurubaran, The Effect of Sodium Alginate on the Properties of Hydroxyapatite. Procedia Eng. **184**, 442–448 (2017). doi:10.1016/j.proeng.2017.04.115
57. P. Chen, L. Liu, J. Pan, J. Mei, C. Li, Y. Zheng, Biomimetic composite composite of hydroxyapatite/gelatin-chitosan core-shell nanofibers for bone tissue engineering. Mater. Sci. Engineering: C **97**, 325–335 (2018). doi:10.1016/j.msec.2018.12.027

58. D. Predoi, S. Iconaru, M. Predoi, M. Motelica-Heino, R. Guegan, N. Buton, Evaluation of Antibacterial Activity of Zinc-Doped Hydroxyapatite Colloids and Dispersion Stability Using Ultrasounds. Nanomaterials **9**(4), 515 (2019). doi:10.3390/nano9040515
59. C.-C. Lin, S.-J. Fu, Y.-C. Lin, I.-K. Yang, Y. Gu, Chitosan-coated electrospun PLA fibers for rapid mineralization of calcium phosphate. Int. J. Biol. Macromol. **68**, 39–47 (2014). doi:10.1016/j.ijbiomac.2014.04.039
60. X. Hong, X. Wu, Q. Zhang, M. Xiao, G. Yang, M. Qiu, G. Han (2012). Hydroxyapatite supported Ag_3PO_4 nanoparticles with higher visible light photocatalytic activity. Appl. Surf. Sci., 258(10), 4801–4805. doi:10.1016/j.apsusc. 2012.01.102
61. M. Manimohan, S. Pugalmani, M.A. Sithique, Synthesis, Spectral Characterisation and Biological Activities of Novel Biomaterial/N, N, O Donor Tridentate Co (II), Ni (II) and Zn (II) Complexes of Hydrazide Based Biopolymer Schiff Base Ligand. J. Inorg. Organomet. Polym Mater. **30**, 4481–4495 (2020). doi:10.1007/s10904-020-01578-7
62. N. Sakthiguru, M. Manimohan, G. Jaganathan, K. Manivannan, M.A. Sithique, Biologically active Chitosan/ZnO/Acalypha indica leaf extract biocomposite: An investigation of antibacterial, cell proliferation and cell migration aptitude for wound healing application. Sustainable Chem. Pharm. **19**, 100357 (2021). doi.org/10.1016/j.scp.2020.100357
63. N. Wang, X. Yu, Q. Kong, Z. Li, P. Li, X. Ren, Z. Deng (2020). Nisin-loaded polydopamine/hydroxyapatite composites: Biomimetic synthesis, and in vitro bioactivity and antibacterial activity evaluations. Colloids Surf., A, 125101. doi:10.1016/j.colsurfa.2020.125101
64. M. Murugaiyan, S.P. Mani, M.A. Sithique, Zinc (ii) centered biologically active novel N, N, O donor tridentate water-soluble hydrazide-based O-carboxymethyl chitosan Schiff base metal complexes: synthesis and characterisation. New J. Chem. **43**, 9540–9554 (2019). doi:10.1039/c9nj00670b
65. O. Geuli, N. Metoki, T. Zada, M. Reches, N. Eliaz, D. Mandler, Synthesis, coating, and drug-release of hydroxyapatite nanoparticles loaded with antibiotics. J. Mater. Chem. B **5**(38), 7819–7830 (2017). doi:10.1039/c7tb02105d
66. Seko, I., Tonbul, H., Tavukçuoğlu, E., Şahin, A., Akbas, S., Yanık, H., … Capan,Y. (2021). Development of curcumin and docetaxel co-loaded actively targeted PLGA nanoparticles to overcome blood brain barrier. Journal of Drug Delivery Science and Technology, 66, 102867. doi: 10.1016/j.jddst.2021.102867
67. A. Jagusiak, K. Chlopas, G. Zemanek, P. Wolski, T. Panczyk, Controlled Release of Doxorubicin from the Drug Delivery Formulation Composed of Single-Walled Carbon Nanotubes and Congo Red: A Molecular Dynamics Study and Dynamic Light Scattering Analysis. Pharmaceutics **12**, 622 (2020). doi:10.3390/pharmaceutics12070622
68. C. Mircioiu, V. Voicu, V. Anuta, A. Tudose, C. Celia, D. Paolino, I. Mircioiu, Mathematical Modeling of Release Kinetics from Supramolecular Drug Delivery Systems. Pharmaceutics **11**(3), 140 (2019). doi:10.3390/pharmaceutics11030140

69. S. Wang, R. Liu, Y. Fu, W.J. Kao, Release mechanisms and applications of drug delivery systems for extended-release. Expert Opin. Drug Deliv. **17**(9), 1289–1304 (2020). doi:10.1080/17425247.2020.1788541
70. R. Jamaledin, P. Makvandi, C.K. Yiu, T. Agarwal, R. Vecchione, W. Sun, P.A. Netti, Engineered microneedle patches for controlled release of active compounds: recent advances in release profile tuning. Adv. Ther. **3**(12), 2000171 (2020). doi:10.1002/adtp.202000171
71. M. Manimohan, S. Pugalmani, K. Ravichandran, M.A. Sithique, Synthesis and characterisation of novel Cu (II)-anchored biopolymer complexes as reusable materials for the photocatalytic degradation of methylene blue. RSC Adv. **10**(31), 18259–18279 (2020). doi:10.1039/d0ra01724h

Scheme

Scheme 1 is available in the Supplementary Files section.

Figures

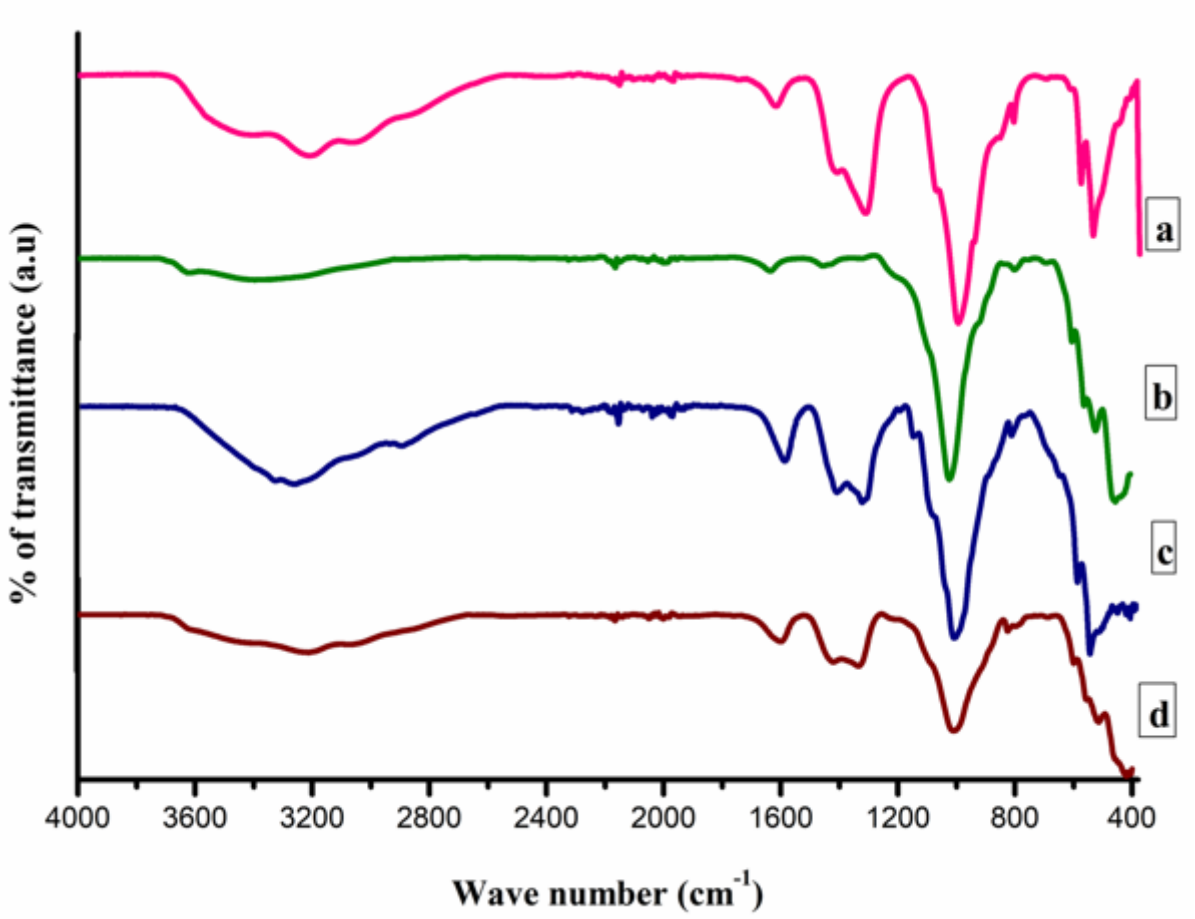

Figure 1

FT-IR spectral analysis of a) HA, b) HA/MMT, c) HA/SA, d) HA/MMT/SA

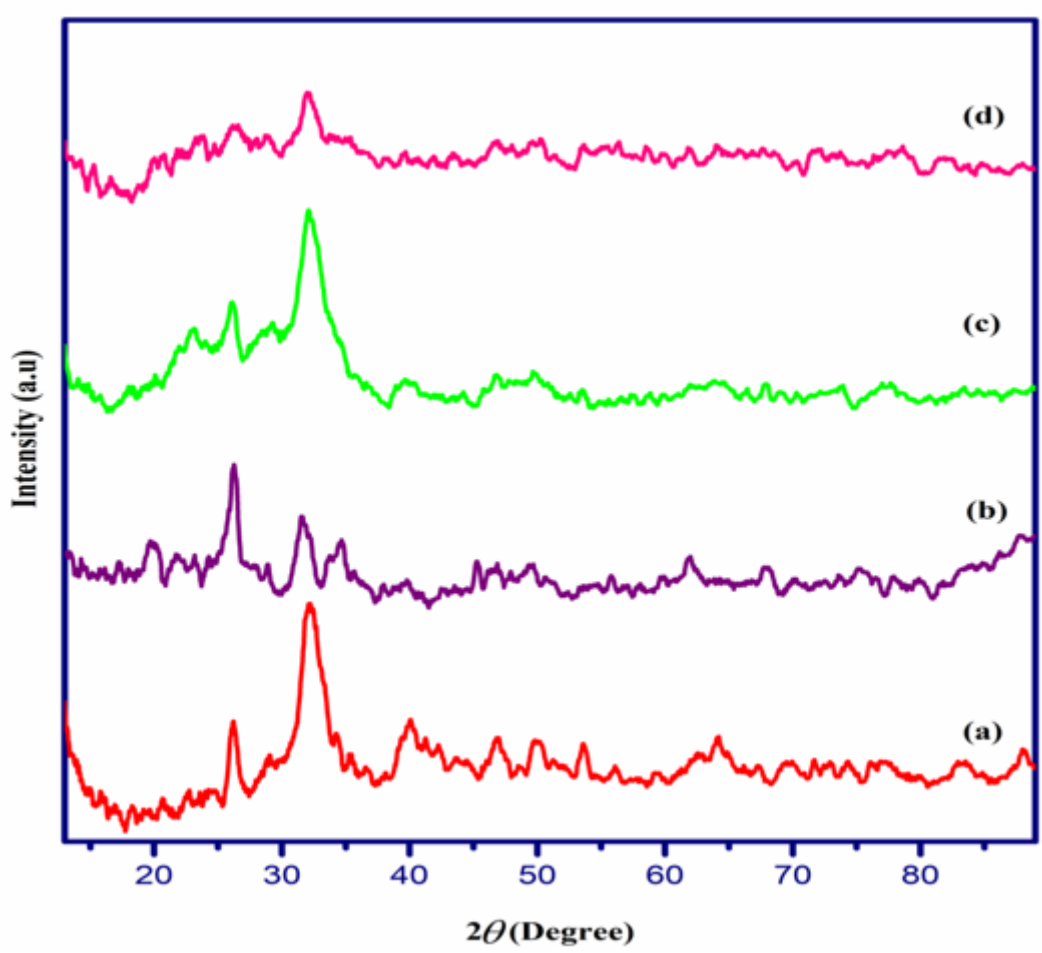

Figure 2

XRD spectral analysis of a) HA, b) HA/MMT, c) HA/SA, d) HA/MMT/SA

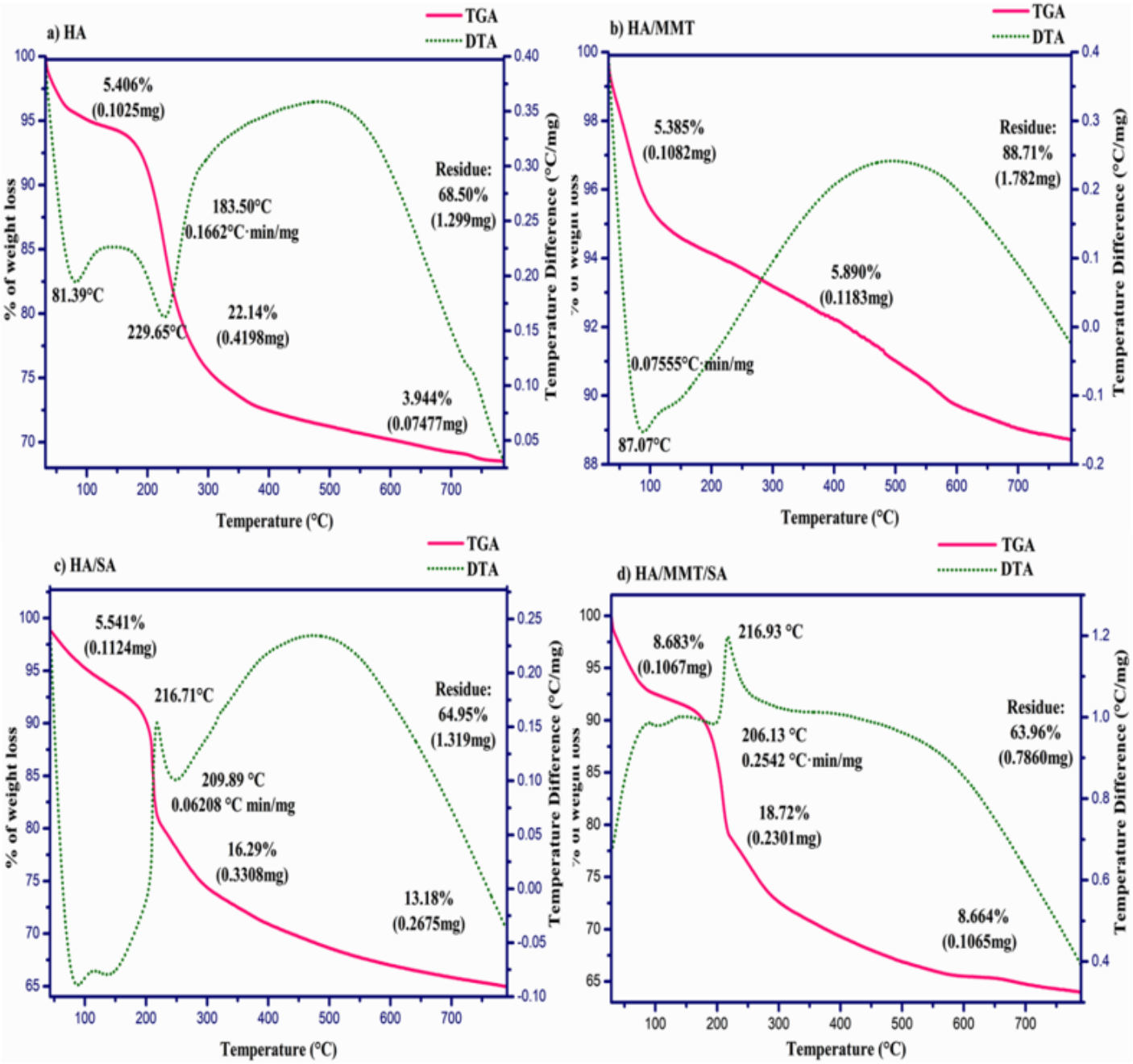

Figure 3

Thermal analysis of a) HA, b) HA/MMT, c) HA/SA, d) HA/MMT/SA

Figure 4

SEM images of a) HA, b) HA/MMT, c) HA/SA, d) HA/MMT/SA

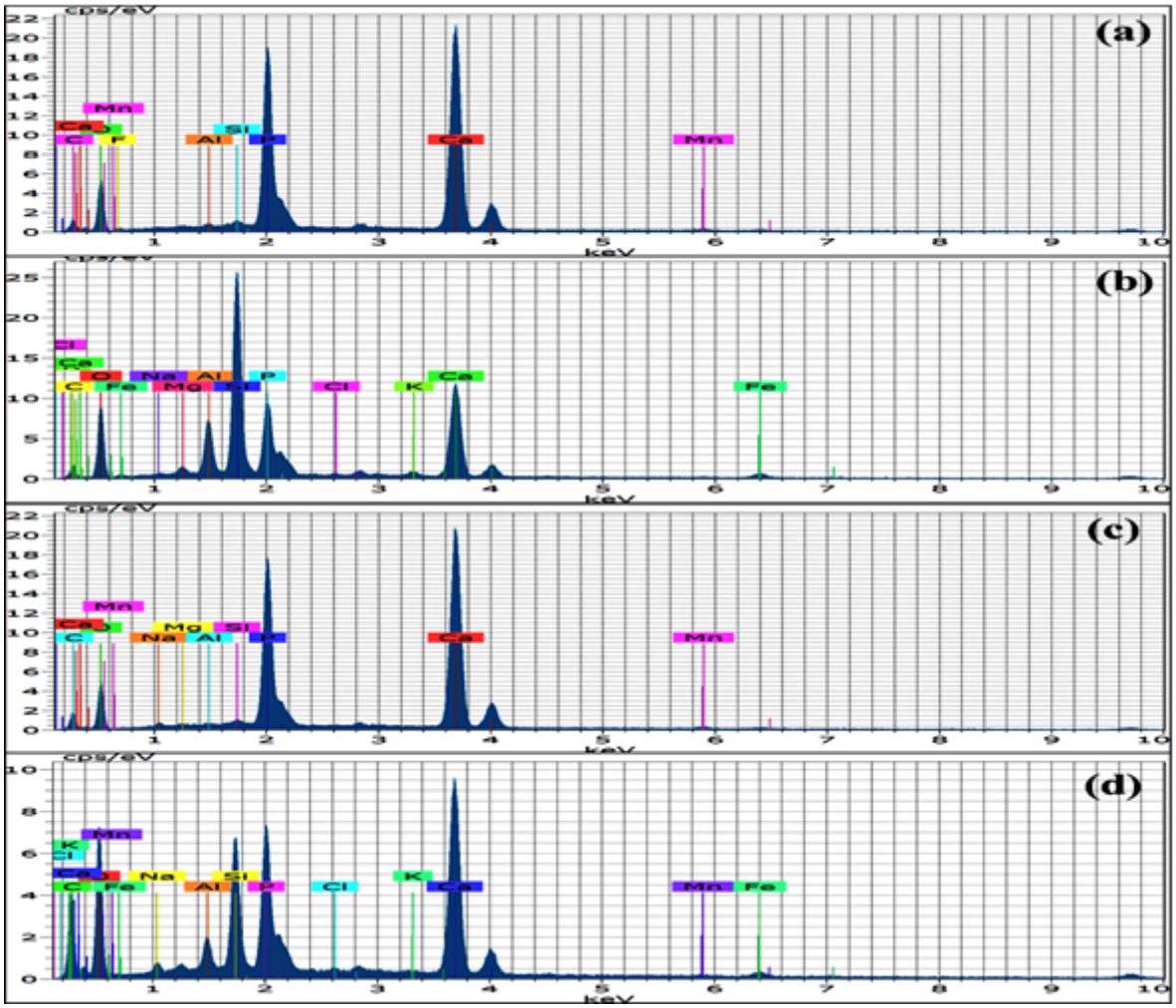

Figure 5

EDAX spectra of a) HA, b) HA/MMT, c) HA/SA, d) HA/MMT/SA

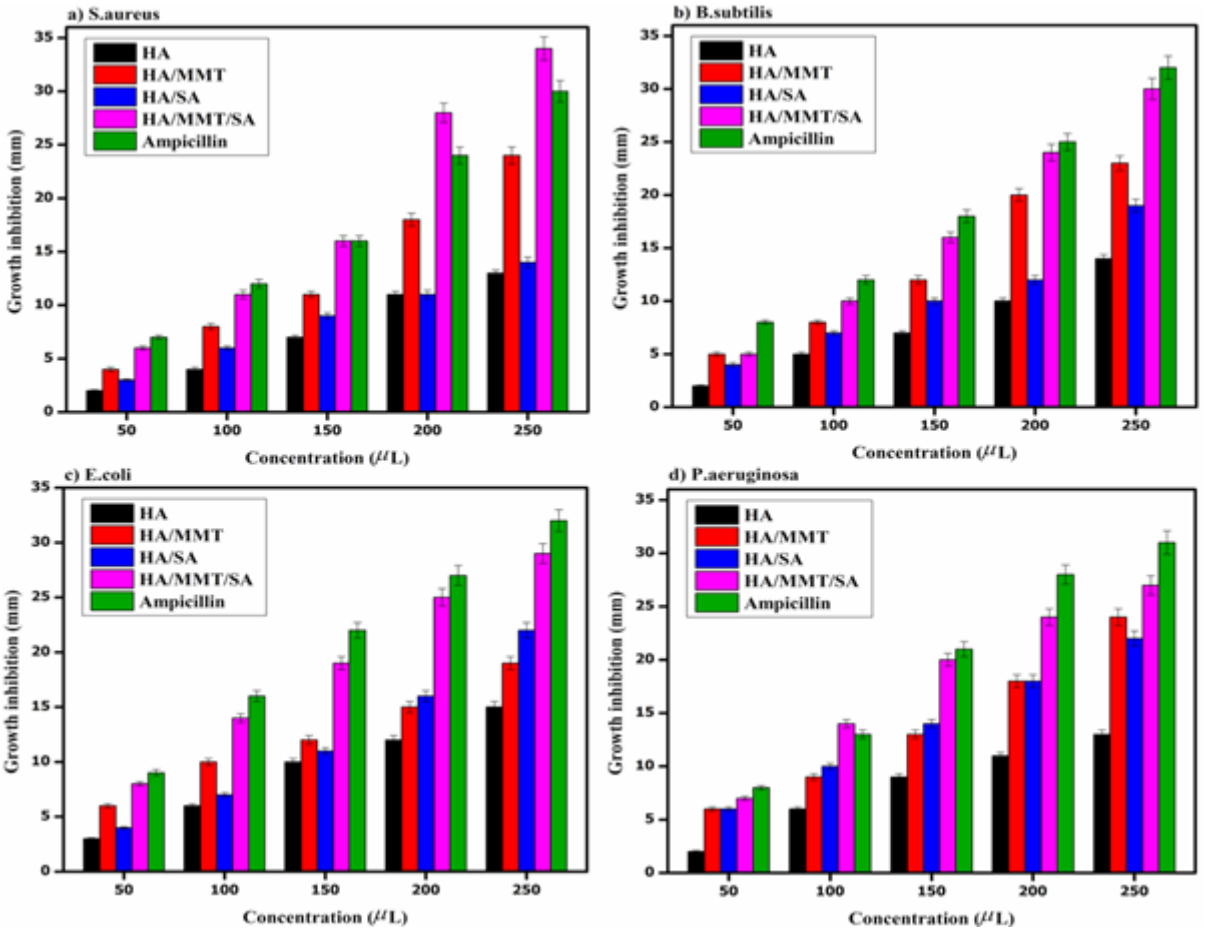

Figure 6

Antibacterial activities of prepared HA and their polymer composites a) S.aureus, b) B.subtilis, c) E.coli, d) P.aeruginosa.

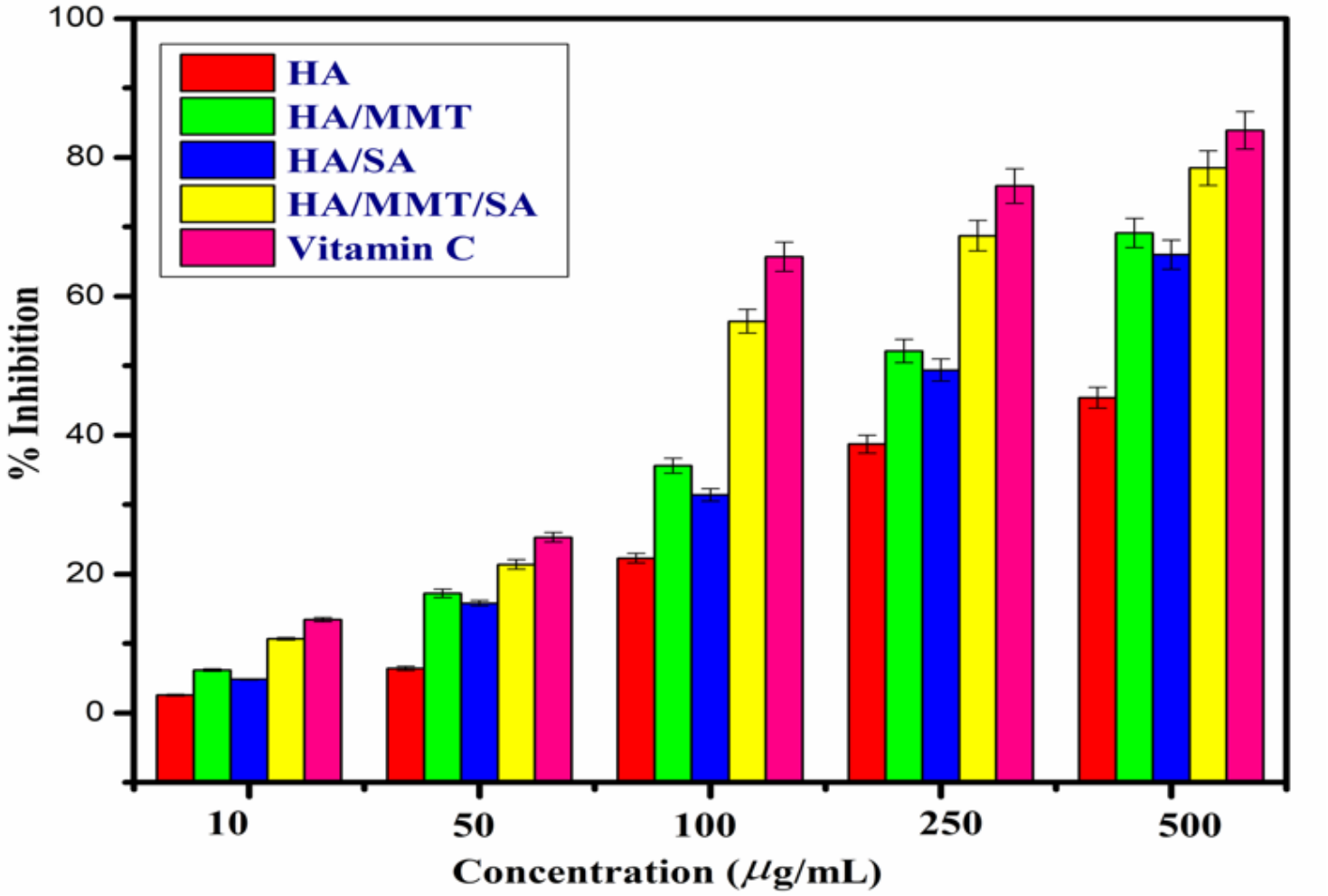

Figure 7

Total antioxidant activities of prepared HA and their hybrid composites.

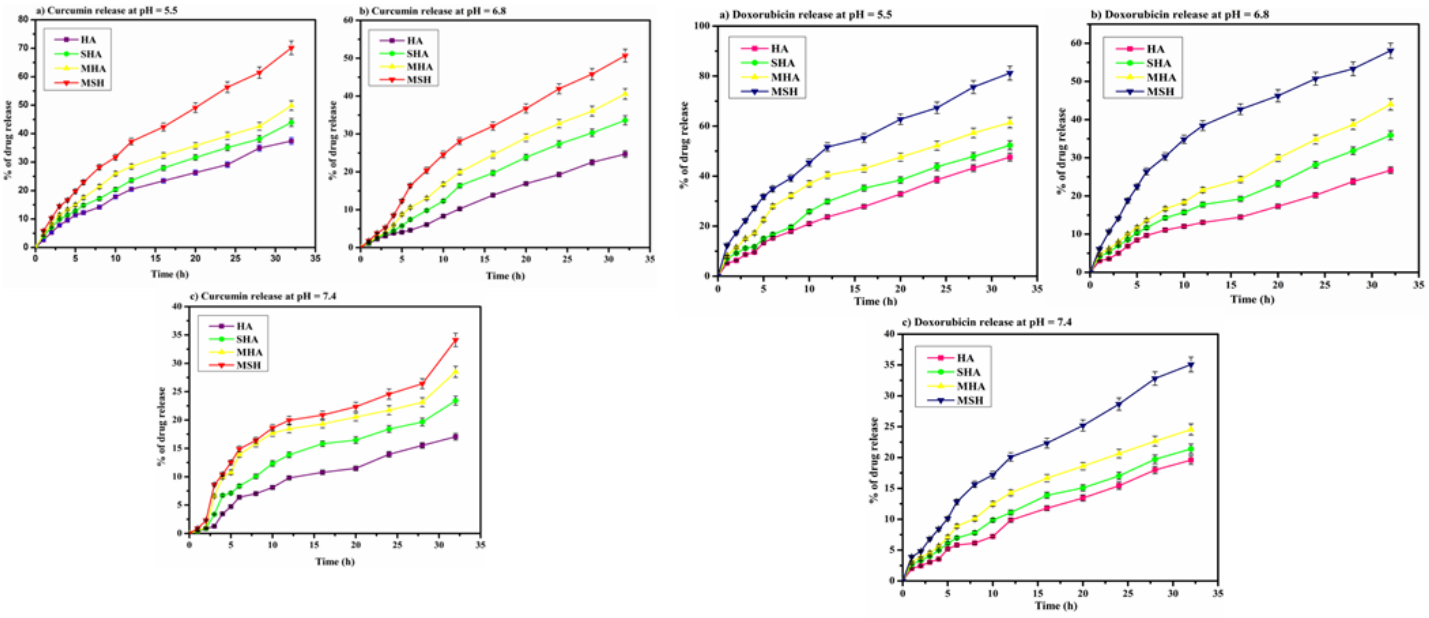

Figure 8

a. Curcumin drug release a) at pH=5.5, b) at pH=6.8, c) at pH=7.4

b. Doxorubicin drug release a) at pH=5.5, b) at pH=6.8, c) at pH=7.4

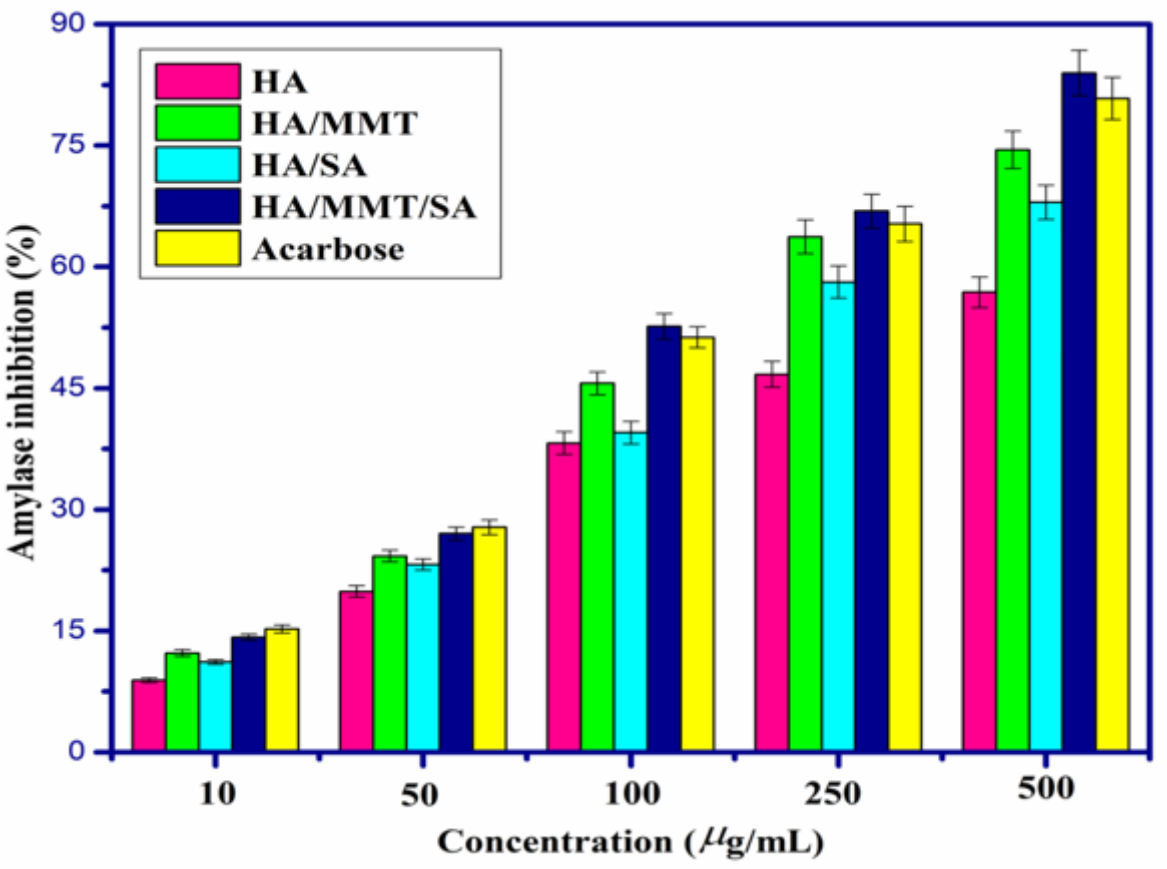

Figure 9

Antidiabetic efficacy of prepared HA and their composite.

Supplementary Files

This is a list of supplementary files associated with this preprint. Click to download.

- GraphicalAbstract.png
- Scheme1.png
- SupplementaryMaterial.docx